Incorporating CT prior information in the robust fuzzy C-means algorithm for QSPECT image segmentation

Chen, Junyu, Jha, Abhinav, Frey, Eric

Junyu Chen, Abhinav K. Jha, Eric C. Frey, "Incorporating CT prior information in the robust fuzzy C-means algorithm for QSPECT image segmentation," Proc. SPIE 10949, Medical Imaging 2019: Image Processing, 109491W (15 March 2019); doi: 10.1117/12.2506805

SPIE.

Event: SPIE Medical Imaging, 2019, San Diego, California, United States

Incorporating CT prior information in the robust fuzzy C-means algorithm for QSPECT image segmentation

Junyu Chen[a], Abhinav K. Jha[b], and Eric C. Frey[a*]

[a]Johns Hopkins University, Baltimore, MD, USA
[b]Washington University in St. Louis, St. Louis, MO, USA

ABSTRACT

Bones are a common site of metastases in a number of cancers including prostate and breast cancer. Assessing response or progression typically relies on planar bone scintigraphy. However, quantitative bone SPECT (BQSPECT) has the potential to provide more accurate assessment. An important component of BQSPECT is segmenting lesions and bones in order to calculate metrics like tumor uptake and metabolic tumor burden. However, due to the poor spatial resolution, noise, and contrast properties of SPECT images, segmentation of bone SPECT images is challenging. In this study, we propose and evaluate a fuzzy C-means (FCM) clustering based semi-automatic segmentation method on quantitative Tc-99m MDP quantitative SPECT/CT. The FCM clustering algorithm has been widely used in medical image segmentation. Yet, the poor resolution and noise properties of SPECT images result in sub-optimal segmentation. We propose to incorporate information from registered CT images, which can be used to segment normal bones quite readily, into the FCM segmentation algorithm. The proposed method modifies the objective function of the robust fuzzy C-means (RFCM) method to include prior information about bone from CT images and spatial information from the SPECT image to allow for simultaneously segmenting lesion and bone in BQSPECT/CT images. The method was evaluated using realistic simulated BQSPECT images. The method and algorithm parameters were evaluated with respect to the dice similarity coefficient (DSC) computed using segmentation results. The effect of the number of iterations used to reconstruct the BQSPECT images was also studied. For the simulated BQSPECT images studied, an average DSC value of 0.75 was obtained for lesions larger than 2 cm^3 with the proposed method.

Keywords: Fuzzy c-means, Image segmentation, SPECT

1. INTRODUCTION

While there has been substantial work on segmentation for other image modalities, there has been limited work for SPECT.[1,2] Segmenting SPECT/CT images is challenging due to the poor spatial resolution and noise properties of SPECT images.[1] As a result, manual segmentation is mostly commonly used clinically, resulting in intra- and inter-observer bias and variability. This work aims at developing a semi-automated method of classifying voxels into soft-tissue, lesion, and bone in quantitative bone SPECT (BQSPECT) images. The research is part of our efforts on developing improved methods for bone and tumor segmentation in patients with bone metastases.[2] The method we propose here is based on the fuzzy C-means (FCM) algorithm for identifying clusters of voxels belonging to the same structures. The noise and resolution properties of the images result in substantial classification errors when applying FCM to SPECT images. The Robust FCM (RFCM) method improves on this by incorporating spatial information that accounts for the cluster distribution in the surrounding voxels.[3] However, we observed that the RFCM method was not successful in classifying bone voxels. We thus propose to augment the spatial information in the SPECT images with anatomical information from registered low-dose CT images. Such CT images are routinely acquired for anatomical localization and to provide an attenuation map when patients are imaged with SPECT/CT systems. The proposed algorithm, Robust fuzzy C-means with prior information (RFCM-p), incorporates the CT information via a prior function. In particular, a term was added to the RFCM objective function to penalize the segmentation differences between CT and

*Corresponding author

Medical Imaging 2019: Image Processing, edited by Elsa D. Angelini, Bennett A. Landman, Proc. of SPIE
Vol. 10949, 109491W · © 2019 SPIE · CCC code: 1605-7422/19/$18 · doi: 10.1117/12.2506805

SPECT image segmentation. We investigated 2 proposed methods for adding the prior information: RFCM-p1 and RFCM-p2. Our proposed RFCM-p1 method incorporates a soft-membership prior; RFCM-p2 method incorporates a hard-membership prior information that is taken from the clustered CT image.

A flow chart of the proposed algorithm is shown is shown in figure 1. A 3D region of interest (ROI) and seed pixels are selected prior to the segmentation process. The segmentation is performed only within this ROI. The seed voxels are used in the region growing algorithm and not in the clustering, as described below. During the segmentation process, bone segmentation is first obtained by applying a binary region growing method on a label map that is clustered by the RFCM. Then, the segmented bone regions are used as prior information in the RFCM-p2 method for clustering the SPECT image. In the last step, a binary region growing method is applied to obtain the final segmentation of the bone and the lesion regions in SPECT image. The region growing algorithm checks 26-connected neighbors of the seed voxels to determine whether they should be included in segmented region containing the seed voxel. Figure 2 shows an example slice of a selected 3D ROI in the CT and SPECT image.

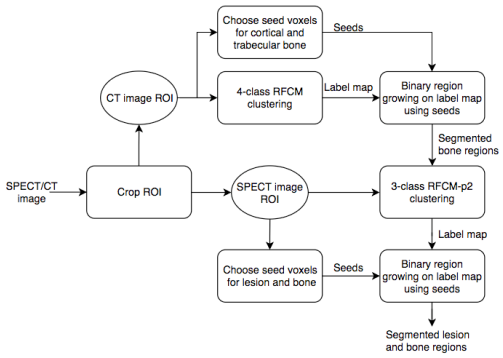

Figure 1: Overview of algorithmic pipeline.

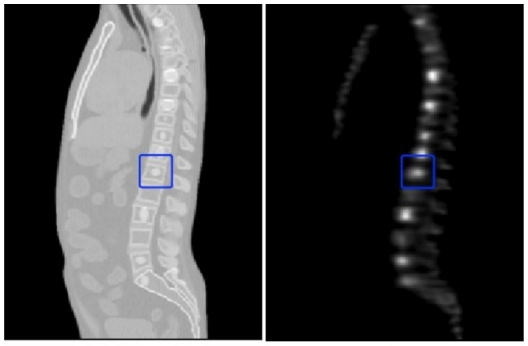

Figure 2: Images (a) and (b) contain an example sagittal slice of 3D ROI selection in the CT (left) and the SPECT (right) images.

2. METHODS

2.1 The conventional FCM algorithm

FCM clustering algorithm was proposed by Bezdek in 1984; it is an improvement of the hard membership K-means algorithm.[4] The algorithm assigns membership of each cluster to a given voxel, depending on the similarity of the voxel intensity value to a particular cluster relative to all other clusters. Similar to K-means, FCM is an iterative optimization algorithm that minimizes the objective function:

$$J_{FCM} = \sum_{j\in\Omega}\sum_{k=1}^{C} u_{jk}^{q}\|y_j - v_k\|^2, \tag{1}$$

where Ω is the image domain, C is the number of classes, u represents the membership function, y_j is the observation at j^{th} voxel, v_k is the centroid of k^{th} class, and the parameter q is a weighting exponent that satisfies $q > 1$ and it controls the amount of fuzzy overlap between clusters.[4] Larger q values allow for a greater degree of overlap between the voxel values in clusters(and vice versa). The optimization problem of objective function is given by:

$$\min_{u_{jk},v_k} J_{FCM}, \quad s.t. \begin{cases} \sum_{k=1}^{C} u_{jk} = 1, & \forall j \in \Omega \\ 0 < \sum_{j\in\Omega} u_{jk} < N, & k = 1, ..., C \end{cases}. \tag{2}$$

When J_{FCM} is minimized, the larger membership values are assigned to voxels where the observations are closer to the class centroid, and lower membership values are assigned to voxels where the observations are further from the class centroid.

2.2 The robust FCM algorithm

The objective function of conventional FCM algorithm in 1 does not take into consideration any spatial information. Thus, the membership functions can be affected by noise, producing a noisy clustering (i.e., clustering where there are voxels with vastly different membership function values than all their neighbors). The RFCM was developed to overcome this shortcoming by adding a spatial smoothness term. The new objective function is defined as:[3]

$$J_{RFCM} = \sum_{j\in\Omega}\sum_{k=1}^{C} u_{jk}^{q}\|y_j - v_k\|^2 + \frac{\beta}{2}\sum_{j\in\Omega}\sum_{k=1}^{C} u_{jk}^{q}\sum_{l\in N_j}\sum_{m\in M_k} u_{lm}^{q}, \tag{3}$$

Here, the term N_j denotes the 26-connected neighbors of the j^{th} voxel, M_k represents the classes $\{1, ..., C\} \setminus \{k\}$ (i.e., classes other than k), and β controls the weight of spatial smoothness term. The spatial smoothness term constrains the membership value of a class to be negatively correlated with the membership values of the other classes in neighboring pixels.[3]

2.3 RFCM algorithm with prior information

Our first proposed method, RFCM-p1, is based on a new formulation of the objective function of the RFCM algorithm to incorporate the CT prior information. By introducing a new regularizing term, the new objective function can be written as:

$$J_{RFCM-p1} = \sum_{j\in\Omega}\sum_{k=1}^{C} u_{jk}^{q}\|y_j - v_k\|^2 + \frac{\beta}{2}\sum_{j\in\Omega}\sum_{k=1}^{C} u_{jk}^{q}\sum_{l\in N_j}\sum_{m\in M_k} u_{lm}^{q} + \gamma\sum_{j\in\Omega}\sum_{k=1}^{C} u_{jk}^{q}\sum_{m\in M_k}(u_{jm}^{(CT)})^{q}, \tag{4}$$

in the new regularizing term, the membership function $u^{(CT)}$ is obtained by applying the RFCM algorithm to the CT image. The new term penalizes the differences between the segmentation obtained using the CT and the SPECT images, and the strength of the penalty is controlled by the parameter γ. Note that when $\beta = 0$ and $\gamma = 0$, the equation 4 is identical to the objective function of the conventional FCM (1). By applying the Lagrange multiplier method to minimize $J_{RFCM-p1}$, an iterative algorithm for computing u_{jk} and v_k can be obtained:

$$u_{jk} = \frac{(\|y_j - v_k\|^2 + \beta\sum_{l\in N_j}\sum_{m\in M_k} u_{lm}^{q} + \gamma\sum_{m\in M_k}(u_{jm}^{(CT)})^{q})^{\frac{-1}{q-1}}}{\sum_{i=1}^{C}(\|y_j - v_i\|^2 + \beta\sum_{l\in N_j}\sum_{m\in M_i} u_{lm}^{q} + \gamma\sum_{m\in M_i}(u_{jm}^{(CT)})^{q})^{\frac{-1}{q-1}}} \tag{5}$$

and

$$v_k = \frac{\sum_{j\in\Omega} u_{jk}^{q} y_j}{\sum_{j\in\Omega} u_{jk}^{q}}. \tag{6}$$

When minimizing the objective function, the new regularizing term tends to increase the u_{jk} when the CT membership value of other classes (i.e. $u_{jm}^{(CT)}$, where $m \in \{\text{classes}\}\backslash\{k\}$) is small and encourages the membership values in each voxel to be similar to the CT membership values in the corresponding CT voxel.

Note that RFCM-p1 requires the number of classes in u_{jk} to be the same as in $u_{jm}^{(CT)}$. Yet, the number of classes in SPECT and CT images might be different. In case of bone imaging, the CT image of bone contains four classes (soft tissue, cortical bone, trabecular bone, and bone lesion), but in SPECT images only three classes are readily identified (soft tissue, bone, bone lesion): Because of the low spatial resolution, SPECT usually cannot differentiate cortical bone and trabecular bone. Merging soft membership values of different classes requires some post-processing on the membership function. A trivial solution is to combine hard membership functions (labels). The next subsection explains the process of combining hard memberships of cortical bone and trabecular bone as one type. Alternatively, the regularizing term can be modified to incorporate hard memberships, $z^{(CT)}$, of the clustered CT image. The objective function of our second proposed method, RFCM-p2, is defined as:

$$J_{RFCM-p2} = \sum_{j\in\Omega}\sum_{k=1}^{C} u_{jk}^{q}\|y_j - v_k\|^2 + \frac{\beta}{2}\sum_{j\in\Omega}\sum_{k=1}^{C} u_{jk}^{q}\sum_{l\in N_j}\sum_{m\in M_k} u_{lm}^{q} + \gamma\sum_{j\in\Omega}\sum_{k=1}^{C} u_{jk}^{q}\sum_{m\in M_k}(z_{jm}^{(CT)})^{q}, \tag{7}$$

where $z^{(CT)}$ is defined as:

$$z_{jk}^{(CT)} = \begin{cases} 1, \text{if voxel } j \text{ is in class } k \\ 0, \text{otherwise} \end{cases}. \tag{8}$$

Minimizing $J_{RFCM-p2}$ with the Lagrange multiplier method yields:

$$u_{jk} = \frac{(\|y_j - v_k\|^2 + \beta\sum_{l\in N_j}\sum_{m\in M_k} u_{lm}^{q} + \gamma\sum_{m\in M_k}(z_{jm}^{(CT)})^{q})^{\frac{-1}{q-1}}}{\sum_{i=1}^{C}(\|y_j - v_i\|^2 + \beta\sum_{l\in N_j}\sum_{m\in M_i} u_{lm}^{q} + \gamma\sum_{m\in M_i}(z_{jm}^{(CT)})^{q})^{\frac{-1}{q-1}}}, \tag{9}$$

and v_k remains the same as equation 6.

Since the objective function likely has local minima, and the algorithm is not guaranteed to be globally convergent, the choice of initial conditions is important. In the proposed method, instead of generating random initial centroids v_k, the initial guess for each cluster center v_k is obtained using the K-means clustering algorithm. The intensity values were normalized before executing the clustering algorithm. The convergence of the algorithm was judged based on changes in the cluster centroid or the membership function at two successive iterations.

2.4 Extract clustered regions in CT

Seed voxels were used to provide information to identify cortical and trabecular bone clusters in the CT image. In the consideration of the discontinuity of bone structures in space, all regions that contain the class label of the seed voxel of the bone were identified as segmented bone regions. Finally, the label maps of cortical and trabecular bone regions were merged, as shown in Figure 3, to form the bone region.

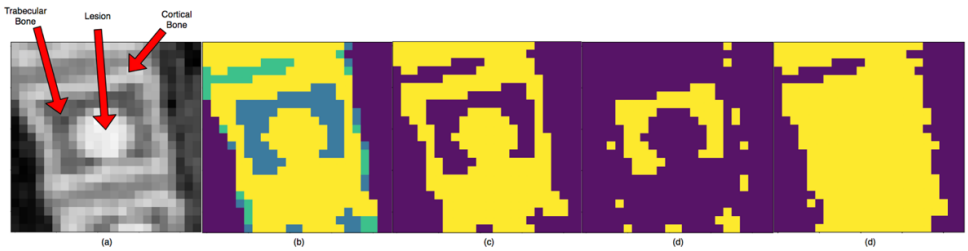

Figure 3: (a) shows the cropped 2D slice of the 3D CT image. (b) displays an example of clustering result by RFCM. (c) and (d) contains the segmentation results for cortical bone and trabecular bone respectively. (e) shows the combined label map of bone.

2.5 Extract clustered regions in SPECT

2.5.1 Extract regions that have the same label as seed voxel (Bone segmentation)

We applied the same strategy discussed above to extract bone regions from clustered QSPECT images.

2.5.2 Extract regions that have the same label as seed voxel (Lesion segmentation)

We used the binary region growing method described in [5] to identify the final lesion regions. Due to noise, the seed voxel may be falsely classified as part of some other class. To ensure the correctness of the seed voxel, we applied a $3 \times 3 \times 3$ cubic box around the seed voxel. The lesion label of the seed was changed to the class that had maximum number of voxels in the cubic box surrounding the seed voxel. The voxels belonging to this class were then used as the starting points of the region growing method. The algorithm stopped when voxels with different labels were encountered.

2.6 Selection of parameters

The parameters of the algorithm were separately optimized for the CT and SPECT images. The optimal parameters were chosen based on the mean dice similarity coefficients (DSC) over the lesions and noise realizations investigated. We used the following procedure.

- First, for the RFCM algorithm, we found the value of β that produced the highest DSC between the true bone regions and segmented CT bone regions.
- The optimal number of iterations in the generation of SPECT image was chosen based on the best mean DSC of lesion segmentations using RFCM-p2. During this process, we kept γ as 0 and varied β in RFCM-p2.
- The optimal β and γ in RFCM-p2 for segmenting SPECT images with the optimal number of reconstruction iterations for a specific range of lesion sizes were then found.

2.7 Image simulation

The basis for the simulation were 3D activity and attenuation distributions based on the realistic NURBS-based XCAT phantom.[6] Attenuation values were computed based on the material compositions of the materials and the attenuation coefficients of the constituents at 140 keV, the photon energy of Tc-99m. The bones had an uptake of 10 times the soft-tissue background. Sclerotic bone lesions with increased attenuation coefficient and radio-pharmaceutical uptake were modeled. Seventy-three bone lesions with sizes ranging from 0.2 to 0.5 cc, uptakes ranging from 3.5-4.5 times that of normal bone, and attenuation coefficients from 13-37% greater than normal bone were modeled.

CT images used in this study were simulated by adding Poisson distributed noise to the attenuation map of the phantom to model a low-dose CT acquisition. SPECT projections were simulated using an analytic projection algorithm that realistically models attenuation, scatter, and the spatially-varying collimator-detector response.[7,8] A total of 50 independent noise realizations were generated. BQSPECT images were reconstructed from these using a quantitative image reconstruction method[9] based on the ordered subsets expectation-maximization algorithm[10] (OS-EM). A total of 1 simulated CT image and 350 simulated SPECT (50 noise realizations from each of iterations 1, 2, 5, 10, 20, 30 and 40) images were used to evaluate the methods

3. RESULTS

Due to the different number of classes in the CT and BQSPECT clustering, we only applied and evaluated the RFCM-p2 algorithm. The algorithms were applied to three dimensional CT and SPECT image; a twenty-six voxel neighborhood system was used for the spatial smoothness term. For segmenting the CT volume, $q = 2$ and $C = 4$ were used in RFCM, where the four classes corresponded to soft tissue, cortical bone, trabecular bone, and lesion; For segmenting SPECT volume, $q = 2$ and $C = 3$ were used in RFCM-p2, where three classes were soft tissue, bone, and lesion.

Figure 4 shows examples of the original BQSPECT and CT images; The red and green curves in the images represent true bone and lesion region outlines, respectively. Figure 5a shows the true bone regions in that slice; figures 5b-5d show segmented bone regions in CT image using RFCM with $\beta = 0$, 0.005, and 0.01, respectively. As β increases, the outlines of the segmented bone regions become smoother. Figures 6a-6d present segmented BQSPECT images with $\beta = 0.0005$ and $\gamma = 0.005$, 0.01, and 0.05 respectively from the RFCM-p2 algorithm, where the red curves indicate segmented bone regions and green curves indicate segmented lesion regions. The resulting images suggest that as gamma increases the differences between segmented bone regions from SPECT and CT images become smaller.

In all cases, the segmentation results were compared to the lesion and bone ground truth labels, which were known for this realistic simulated data. As shown in Figures 7 and 8, the optimal β for RFCM CT bone segmentation was 0.0064, and the optimal number of reconstruction iterations was 2 for the RFCM-p2 segmentation of the BQSPECT images. Table 1 shows the β and γ values and corresponding evaluated DSC values for different ranges of lesion sizes averaged over the 50 different noise realizations. The standard deviation of the DSC values for the various size rangers were calculated from the 50 noise realizations. DSC larger than 0.7 were obtained for lesion sizes larger than 2 cm^3, which may be regarded as a good segmentation result.[11,12]

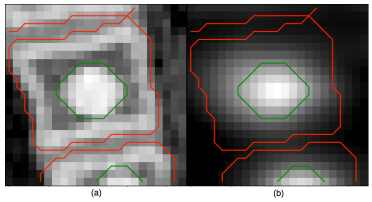

Figure 4: Image (a) shows the CT image. (b) shows the SPECT image (2 iterations). Red contours indicate bone ground truth and green contours indicate lesion ground truth.

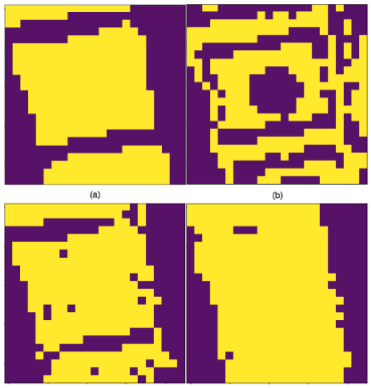

Figure 5: Yellow regions in all images represent bone regions. (a) shows the ground truth bone region. (b), (c), and (d) show segmented bone regions from the CT image with $\beta = 0$, 0.0005, and 0.001 respectively.

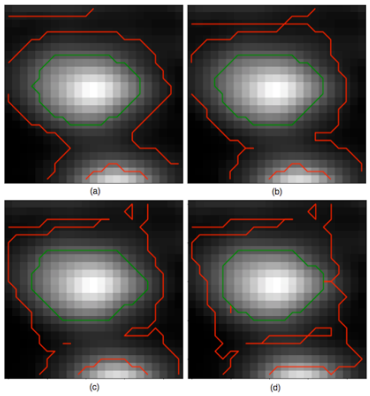

Figure 6: Red contours in the images represent segmented bone regions and green contours indicate lesion regions. The segmentation result in image (a) was obtained with $\beta = 0.0005$ and $\gamma = 0$. The segmentation results in images (b), (c), and (d) were obtained with $\beta = 0.0005$ and $\gamma = 0.005$, 0.01, and 0.05, respectively.

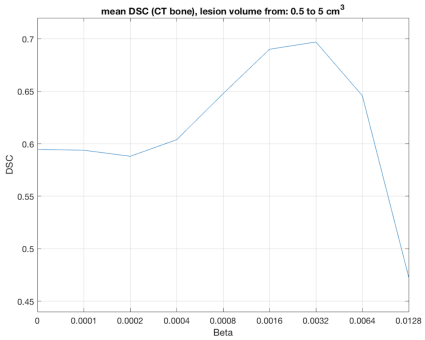

Figure 7: Mean over lesions (0.5 to 5 cc in lesion volume) of DSC values as a function of β for the RFCM method used to segment the CT images.

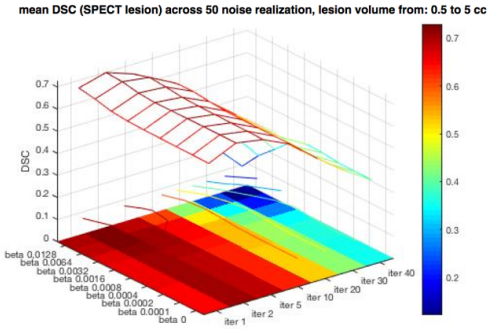

Figure 8: Mean DSC over all lesions with volumes 0.5 to 5 cc and noise realizations as a function of the iteration number and β for the RFCM-p2 method applied to the SPECT images using the class labels from the RFCM segmentation of the CT images obtained using the value of β that gave the highest DSC in Figure 7.

4. CONCLUSION

Because of their challenging noise and resolution characteristics, there has been limited work on segmentation of SPECT images.[15] The proposed work presents a novel semi-automatic 3D approach for segmenting bone and lesion in BQSPECT images. The proposed RFCM-pn algorithms is a modified RFCM clustering algorithm to incorporate prior information from CT images; it is also suitable for clustering other multi-modality images, such as PET/CT and PET/MRI. The new penalty functions can also be readily applied to other variants of FCM, such as FCM_S[13] and FLICM[14]. In this paper, we discussed the application of the algorithm on the simultaneous segmentation of the bone lesion and bone structures in the context of quantitative Tc-99m MDP QSPECT/CT images. The resulting DSC values reported in this paper show that the proposed approach is an effective method for lesion and bone segmentation in BQSPECT images for lesions larger than 2 cc in volume. The results also suggest that RFCM-p algorithm is suitable for performing image clustering on any multi-modality images.

Lesion size (cm^3)	β	γ	Avg. DSC (lesion)	Avg. DSC (bone)
4-5	0.0001	0.004	0.785 ($\pm$ 0.026)	0.777 ($\pm$ 0.008)
3-4	0.0016	0.002	0.747 ($\pm$ 0.030)	0.820 ($\pm$ 0.023)
2-3	0.0002	0.008	0.717 ($\pm$ 0.018)	0.709 ($\pm$ 0.030)
1-2	0.0004	0.001	0.618 ($\pm$ 0.010)	0.647 ($\pm$ 0.026)
0-1	0.0016	0.064	0.512 ($\pm$ 0.016)	0.637 ($\pm$ 0.020)

Table 1: Results for SPECT images reconstructed with 2 iterations (12 subsets) in terms of the highest average DSC and corresponding lesion size, β, and γ values.

ACKNOWLEDGMENTS

This work was supported by a grant from the National Cancer Institute, U01-CA140204. The views expressed in written conference materials or publications and by speakers and moderators do not necessarily reflect the official policies of the NIH; nor does mention by trade names, commercial practices, or organizations imply endorsement by the U.S. Government.

REFERENCES

[1] Gustafsson, J., Sundlöv, A., and Sjögreen Gleisner, K., "SPECT image segmentation for estimation of tumour volume and activity concentration in 177Lu-DOTATATE radionuclide therapy," *EJNMMI Research* **7**(1) (2017).

[2] Jha, A., Rowe, S., Du, Y., and Frey, E. C., "An unsupervised semi-automated segmentation technique to delineate tumors and bones in SPECT images of patients with bone metastasis," *The Journal of Nuclear Medicine* **58** (2017).

[3] Pham, D. L., "Spatial Models for Fuzzy Clustering," *Computer Vision and Image Understanding* **84**, 285–297 (nov 2001).

[4] Bezdek, J. C., Ehrlich, R., and Full, W., "FCM: The fuzzy c-means clustering algorithm," *Computers & Geosciences* **10**, 191–203 (jan 1984).

[5] Jha, A. K., Rodriguez, J. J., Stephen, R. M., and Stopeck, A. T., "A clustering algorithm for liver lesion segmentation of diffusion-weighted MR images," in [*2010 IEEE Southwest Symposium on Image Analysis & Interpretation (SSIAI)*], 93–96, IEEE (may 2010).

[6] Segars, W. P., Mahesh, M., Beck, T. J., Frey, E. C., and Tsui, B. M. W., "Realistic ct simulation using the 4d xcat phantom," *Medical Physics* **35**(8), 3800–3808 (2008).

[7] Frey, E. C. and Tsui, B. M. W., "A practical method for incorporating scatter in a projector-backprojector for accurate scatter compensation in spect," *IEEE Transactions on Nuclear Science* **40**, 1107–1116 (Aug 1993).

[8] Kadrmas, D. J., Frey, E. C., and Tsui, B. M. W., "An svd investigation of modeling scatter in multiple energy windows for improved spect images," *IEEE Transactions on Nuclear Science* **43**, 2275–2284 (Aug 1996).

[9] He, B., Du, Y., Song, X., Segars, W. P., and Frey, E. C., "A Monte Carlo and physical phantom evaluation of quantitative In-111 SPECT," *Physics in Medicine and Biology* **50**, 4169–4185 (Sep 2005).

[10] Hudson, H. M. and Larkin, R. S., "Accelerated image reconstruction using ordered subsets of projection data," *IEEE Transactions on Medical Imaging* **13**, 601–609 (Dec 1994).

[11] Zijdenbos, A., Dawant, B., Margolin, R., and Palmer, A., "Morphometric analysis of white matter lesions in MR images: method and validation," *IEEE Transactions on Medical Imaging* **13**(4), 716–724 (1994).

[12] Bartko, J. J., "Measurement and reliability: statistical thinking considerations.," *Schizophrenia bulletin* **17**(3), 483–9 (1991).

[13] Chen, S. and Zhang, D., "Robust Image Segmentation Using FCM With Spatial Constraints Based on New Kernel-Induced Distance Measure," *IEEE Transactions on Systems, Man and Cybernetics, Part B (Cybernetics)* **34**, 1907–1916 (aug 2004).

[14] Krinidis, S. and Chatzis, V., "A Robust Fuzzy Local Information C-Means Clustering Algorithm," *IEEE Transactions on Image Processing* **19**, 1328–1337 (may 2010).